Electron acoustic instability in four component space plasmas with observed generalized (*r,q*) distribution function

Sumbul Sehar, M. N. S. Qureshi, and H. A. Shah

Electron acoustic instability in four component space plasmas with observed generalized (*r,q*) distribution function

View Online   Export Citation   CrossMark

Sumbul Sehar,[a)] M. N. S. Qureshi, and H. A. Shah [iD]

AFFILIATIONS

Department of Physics, GC University, 54000 Lahore, Pakistan

[a)]Corresponding Author Sumbul Sehar Department of Physics, GC University, Lahore 5400, Pakistan.
E-mail: ssfawa3@hotmail.com

ABSTRACT

Electron acoustic instability in magnetized four component plasma has been studied by employing non-Maxwellian generalized (*r*, *q*) distribution function. We observed electron velocity distribution function using Cluster data and found that the electron distribution contains three components, cool, hot and warm beam (strahl) all showing flat-top nature. By fitting the observed distribution with the generalized (*r*, *q*) distribution, we used the fitting parameters for cool, hot and beam electron components in the numerical results. We have investigated the effect of beam density, beam temperature, beam velocity and propagation angle on the real frequency and growth rate of the electron acoustic waves in strongly magnetized plasma.

I. INTRODUCTION

In space or laboratory plasmas, variety of wave modes and instabilities can be found which further enriched by the presence of different species of electrons and ions. It is believed that space plasmas possess non-Maxwellian distribution which are also responsible for the generation of instabilities. It has been shown that around the Earth's bow shock electron distributions with drifting Maxwellian core and high energy tails can destabilize the electrostatic waves such as electron acoustic and ion acoustic waves.[1,2] Electron acoustic waves (EAWs) are strongly damped in homogeneous and unmagnetized electron-ion Vlasov plasma, however, become physically significant in two electron component plasma.[3] Different temperatures of electron components and relative drifts can produce electron acoustic (EA) instability in the frequency range $\omega_{pi} < \omega_r < \omega_{pe}$, where $\omega_{pi} = \frac{4\pi n_0 e^2}{m_i}$ and $\omega_{pe} = \frac{4\pi n_0 e^2}{m_e}$ are the ion and electron plasma frequencies, respectively.[4] DE-1 satellite data of polar cusp region showed that EAW becomes unstable when the plasma consists of cool electron component $T_c \sim 1\,\mathrm{eV}$, warm electron beam $T_b \sim 20\,\mathrm{eV}$

and hot electron component $T_h \sim 100\,\mathrm{eV}$, where subscript '*c*', '*b*' and '*h*' refer to cool, beam and hot electrons, respectively. Similarly plasma in auroral region composed of cool and hot electron components with temperatures of few eV and 100-200 eV, respectively, a warm drifting electron beam is highly suitable for EA instability.

It was believed that intense electrostatic waves up to the electron plasma frequency can be generated due to Doppler shifted ion acoustic waves upstream of the Earth's bow shock.[5] However, later on it was established that EAWs provide better description for the cusp auroral hiss formation and broadband electrostatic noise (BEN), which have been extensively investigated in literature.[4,6,7] Simulations of EAWs showed that EA instability is responsible for the generation of BEN in polar cusp region.[8-10] Upon classification of wave frequencies related to BEN emission it has been established that it extends from lower hybrid frequency of few Hertz up to electron cyclotron frequency or mostly to the electron plasma frequency.[11] Due to this broad range of frequency it was supposed that numerous modes of plasma are associated with BEN. Satellite measurements confirmed the BEN emission in

different regions of Earth's magnetosphere such as in magnetotail, bow shock, polar cusp and auroral region. The analytical and numerical investigation of modified EA instability in magnetized plasma driven by hot field aligned ion beam shows that EA instability successfully explains BEN generation in magnetotail.[12]

EA instability has been studied in a three component plasma composed of cool electrons, hot electrons and ions, all were treated as unmagnetized, and found that EAWs can propagate in plasma with light damping if $\frac{T_h}{T_c} > 0.1$ and $\frac{n_c}{n_e} < 0.8$, where subscript 'e' refers to total electron population.[13] However, later on it has been showed that if the cool and hot electron components have relative drift several times more than the cool electron thermal speed, both considered as Maxwellian, then EA instability can arise.[14] EA instability driven by field aligned and cross field hot anisotropic electron beam was studied by Bharutharm.[15,16] In field aligned case, it was found that growth of EA instability is highly dependent on beam temperature and density, however in cross field case electron acoustic instability transformed into modified two stream instability. Hellberg et al.[17] reported the experimental observations of EAWs in a two electron component plasma and showed that observed dispersion and damping rates were well explained when hot electrons were modelled by kappa distribution and cool electrons and ions as Maxwellian. Mbuli et al.[18] studied the EA instability in four component magnetized plasma by employing idealistic Maxwellian distribution function for all species.

Since space plasmas often possess non-Maxwellian distributions containing superthermal tails and/or flat tops at low energies. Distributions with high energy tails are well modelled by family of kappa type distribution, however, when distributions contain flat tops or spikes at low energies with or without high energy particles, generalized (r, q) distribution function is the ultimate choice. The first reported observations of flat top electron distributions have been reported by Montgomery et al.[19] by Vela 4 observations. Subsequent observations of electron flat top distributions were also reported across the bow shock[1,20] and around the neutral line in the magnetotail.[21] It is now believed that electron distributions around the bow shock generally exhibit flat tops at low energies.[22] Parks et al.[23] showed that the broadband electrostatic emissions are associated with the flat top electron distributions similar to those observed earlier by Feldman across the bow shock.

In recent years, generalized (r, q) distribution function has successfully been used in numerous simulation and theoretical studies due to its wide range of applications in space plasmas.[24-26] Zaheer and Yoon[27] modelled the solar wind electrons with (r, q) distribution function to see the influence of interaction between flat top electrons with low frequency kinetic Alfven turbulence and high frequency Langmuir turbulence. Observation of Lion roars from the magnetosheath associated with the flat top distributions has successfully been interpreted qualitatively and quantitatively by employing the flat top (r, q) distribution function[28] which

could not be explained earlier when idealized Maxwellian distribution function was employed.[29] Since plasma with distinct electron temperatures is highly favorable for electron acoustic waves and proper kinetic description of such plasma require that actual observed distribution functions should be employed in theoretical studies. Therefore, in this paper we have studied EAW in a four component magnetized plasma which consists of hot electrons, cool electrons and warm electron beam with stationery ions using observed non-Maxwellian distribution function.

II. DISTRIBUTION FUNCTION

In the above mentioned works in which ion-acoustic waves have been investigated, idealized Maxwellian or Maxwellian-kappa distributions were used. In this paper, we employ a non-Maxwellian distribution such as the generalized (r, q) distribution function, which has the form for jth species ($j = i, c, h, b$, where i, c, h, b stand for ions, cold electrons, hot electrons and electron beam (strahl), respectively)

$$f_j(r,q) = \frac{A}{\Psi_{T_{\perp j}}^2 \Psi_{T_{\parallel j}}} \left(1 + \frac{1}{q-1}\left\{\frac{v_\perp^2}{\Psi_{T_{\perp j}}^2} + \frac{(v_\parallel - u_b)^2}{\Psi_{T_{\parallel j}}^2}\right\}^{r+1}\right)^{-q}, \quad (1)$$

where

$$A = \frac{3(q-1)^{-3/2(1+r)}\Gamma(q)}{4\pi\,\Gamma\left(q - \frac{3}{2(1+r)}\right)\Gamma\left(1 + \frac{3}{2(1+r)}\right)}, \quad (2)$$

is the normalization and the modified thermal speeds are

$$\Psi_{T_{\parallel,\perp}} = v_{t_{\parallel,\perp}}\sqrt{\frac{3(q-1)^{-1/(1+r)}\Gamma\left(\frac{3}{2(1+r)}\right)\Gamma\left(q - \frac{3}{2(1+r)}\right)}{\Gamma\left(\frac{5}{2(1+r)}\right)\Gamma\left(q - \frac{5}{2(1+r)}\right)}}. \quad (3)$$

In the above Eqs. (1)–(3) $v_{t_{\parallel,\perp}} = \sqrt{\frac{T_{\perp,\parallel}}{m}}$ is the thermal velocity where perpendicular ($\perp$) and parallel ($\parallel$) directions correspond to the ambient magnetic field or z-direction, Γ is the Gamma function, u_b is the speed of electron beam, m, T, v are the particle's mass, temperature and speed, respectively. In limiting form when $r = 0$ and $q = \kappa + 1$ generalized (r, q) distribution function reduces to the kappa distribution function and when $r = 0$ and $q \to \infty$, it reduces to the classical Maxwellian distribution function. The spectral indices r and q satisfied the conditions such that $q(1 + r) > 5/2$ and $q > 1$ which comes from the definition of temperature for the (r, q) distribution.[28]

A. Observed distribution

On 21st October, 2001 Cluster was traversing through dayside mid-latitude cusp region in the southern hemisphere at ~ 4 R$_E$ (1 R$_E$ ≈ 6400 km). Cluster has two Plasma Electron and Current Experiment (PEACE) sensors on each spacecraft to analyze electron velocity distribution with full 4π solid angle resolution in the energy range 0.7 eV to 26 keV with a time resolution of 4 s.[30] In Fig. 1, solid circles represent the
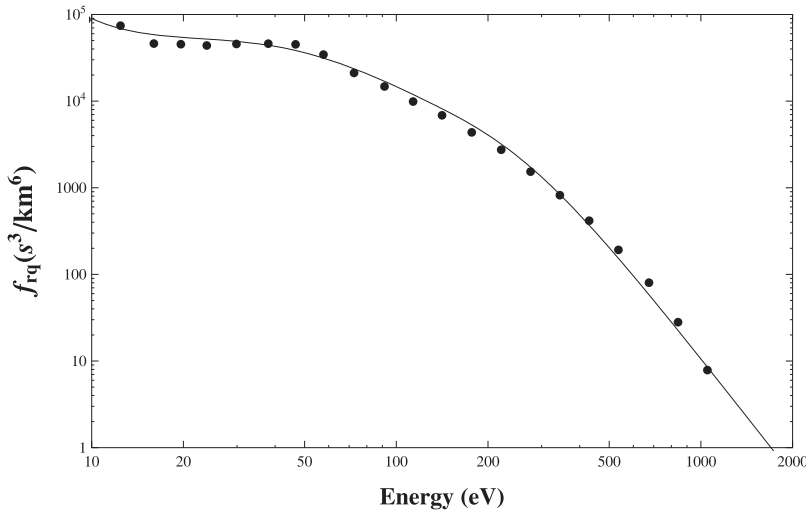
FIG. 1. Electron velocity distribution function observed (solid dots) by Cluster on 21st October, 2001 at 21:11:40 and fitting (solid line) by the generalized (r,q) distribution function. The parameters used in the fitting are n_c = 0.2, $T_{\|c}$ = 3 eV, n_h = 0.5, $T_{\|h}$ = 122 eV, n_b = 0.3, $T_{\|b}$ = 35 eV, r_c = 3.0, q_c = 1.1, r_h = 1.5, q_b = 1.8, r_b = 1.5 and q_b = 1.8.

parallel cut of the observed electron velocity distribution function at 21:11:40 on 21st October, 2001 using PEACE data which is associated with the broadband electrostatic emissions.[23] The solid line in Fig. 1 represents the fitting of the observed distribution function using the generalized (r,q) distribution function given in Eq. (1). Fitting clearly shows that the observed electron distribution has three components; cool, hot and warm beam (strahl) components all show flat-topped nature, with fitting values of density and temperature for each component as n_c = 0.2, $T_{\|c}$ = 3 eV, n_h = 0.5, $T_{\|h}$ = 122 eV and n_b = 0.3, $T_{\|b}$ = 35 eV, respectively. The spectral indices for each component used in the fitting are r_c = 3.0, q_c = 1.1, r_h = 1.5, q_b = 1.8 and r_b = 1.5, q_b = 1.8. The nonzero positive values of spectral index r for each component clearly show that the distribution is a flat top distribution.

III. MATHEMATICAL FORMALISM

In this section, we consider a collisionless, uniform and magnetized plasma consisting of four components, magnetized cool and hot electrons, drifting warm electron beam and stationary ions. We take magnetic field along the z-axis, i.e. $\mathbf{B}_0 = B_0 \hat{e}_z$ and wave vector $\mathbf{k}$ in x-z plane such that $k_z = k_{\|} = k \cos\theta$, $k_x = k_{\perp} = \sin\theta$, and without loss of generality we can take $k_y = 0$ where θ is the angle with the magnetic field direction.

The standard dispersion relation of electrostatic waves in anisotropic, magnetized plasma, satisfying any zeroth order distribution, is[31]

$$1 = 2\pi \sum_j \frac{\omega_{pj}^2}{k^2} \int_0^\infty dv_\perp \, v_\perp \sum_{n=-\infty}^\infty J_n^2\left(\frac{k_\perp v_\perp}{\Omega}\right)$$

$$\times \int_{-\infty}^\infty \left(\frac{n\Omega}{v_\perp}\frac{\partial f_{j0}}{\partial v_\perp} + k_\|\frac{\partial f_{j0}}{\partial v_\|}\right)\frac{dv_\|}{k_\|\left(u_j + v_\|\right) + n\Omega - \omega} \quad (4)$$

Here $\omega_{pj} = \left(4\pi n_{0j}q_j^2/m_j\right)^{1/2}$ is the plasma frequency, $\Omega = qB_0/m_e c$ is the electron cyclotron frequency for electron species, $J_n(z)$ is the Bessel function of the first kind and $z = \frac{k_\perp v_\perp}{\Omega}$ is the argument of the Bessel function. Now by using generalized (r, q) distribution function (1) in above Eq. (4), we get

$$1 = -4A\left(\frac{q(r+1)}{(q-1)}\right)\sum_j \frac{\omega_{pj}^2}{k^2\Psi_{T_{\perp j}}^4}\int_{-\infty}^\infty \left\{1 + \left(1 + \frac{\xi_{nj}}{(s-\xi_{nj})}\right)\left(\frac{T_{\perp j}}{T_{\|j}}-1\right)\right.$$

$$\left. + \left(\frac{\frac{(\omega - k_\| u_j)}{k_\|\Psi_{T_{\|j}}}}{(s-\xi_{nj})}\right)\right\}ds \int_0^\infty v_\perp \sum_{n=-\infty}^\infty J_n^2\left(\frac{k_\perp v_\perp}{\Omega}\right)\left(\frac{v_\|^2}{\Psi_{T_{\|j}}^2} + \frac{v_\perp^2}{\Psi_{T_{\perp j}}^2}\right)^r$$

$$\times \left(1 + \frac{1}{(q-1)}\left(\frac{\left(v_\| - u_j\right)^2}{\Psi_{T_{\|j}}^2} + \frac{v_\perp^2}{\Psi_{T_{\|j}}^2}\right)^{r+1}\right)^{-q-1} dv_\perp \quad (5)$$

where $s = \frac{v_\|}{\Psi_{T_{\|j}}}$ and $\xi_{nj} = \frac{(\omega - n\Omega - k_\| u_j)}{k_\|\Psi_{T_{\|j}}}$. The Bessel function can be separated into following two parts

$$\sum_{n=-\infty}^\infty J_n^2\left(\frac{k_\perp v_\perp}{\Omega}\right) = J_0^2\left(\frac{k_\perp v_\perp}{\Omega}\right) + \sum_{n=1}^\infty J_n^2\left(\frac{k_\perp v_\perp}{\Omega}\right)$$

which can be further simplified by using the identities, $J_0^2\left(\frac{k_\perp v_\perp}{\Omega}\right) = 1$ and

$$J_n^2(z) = J_{-n}^2(z) = \frac{x^{2n}}{n!2^{2n}}\sum_{m=0}^\infty \frac{E_{n,m}}{(n+m)!}\frac{z^{2m}}{m!2^{2m}}$$

where $E_{n,m} = \frac{(-1)^m n![2(n+m)]!}{(2n+m)!(n+m)!}$. So Eq. (5) becomes

$$1 = -4A\left(\frac{q(r+1)}{(q-1)}\right)\sum_j \frac{\omega_{pj}^2}{k^2\Psi_{T_{\perp j}}^4}\int_{-\infty}^{\infty}\left\{1+\left(1+\frac{\xi_{nj}}{(s-\xi_{nj})}\right)\left(\frac{T_{\perp j}}{T_{\|j}}-1\right)\right.$$

$$\left.+\left(\frac{\frac{(\omega-k_\| u_j)}{k_\|\Psi_{T_{\|j}}}}{(s-\xi_{nj})}\right)\right\}ds\int_0^{\infty}v_\perp\left(\frac{v_\|^2}{\Psi_{T_{\|j}}^2}+\frac{v_\perp^2}{\Psi_{T_{\perp j}}^2}\right)^r$$

$$\times\left(1+\frac{1}{(q-1)}\left(\frac{(v_\|-u_j)^2}{\Psi_{T_{\|j}}^2}+\frac{v_\perp^2}{\Psi_{T_{\perp j}}^2}\right)^{r+1}\right)^{-q-1}$$

$$\times\left\{1+\sum_{n=1}^{\infty}\frac{z^{2n}}{n!2^{2n}}\sum_{m=0}^{\infty}\frac{E_{n,m}}{(n+m)!}\frac{z^{2m}}{m!2^{2m}}\right\}dv_\perp \quad (6)$$

After performing integration in the above equation and consider lowest order values of n and m only, i.e. $n=1$ and $m=0$, Eq. (6) can be written in the form as

$$1 = -2A\sum_j\frac{\omega_{pj}^2}{k^2\Psi_{T_{\perp j}}^2}\left[AC_1\frac{T_{\perp j}}{T_{\|j}}+\left(\frac{T_{\perp j}}{T_{\|j}}-1\right)\xi_{0j}Z_1^{(r,q)}(\xi_{0j})\right.$$

$$+\left(\frac{(\omega-k_\| u_j)}{k_\|\Psi_{T_{\|j}}}\right)Z_1^{(r,q)}(\xi_{0j})+\frac{k_\perp^2\Psi_{T_{\|j}}^2}{2\Omega_j^2}\left\{ABC_2\frac{T_{\perp j}}{T_{\|j}}\right.$$

$$+\left(\frac{T_{\perp j}}{T_{\|j}}-1\right)\xi_j Z_2^{(r,q)}(\xi_j)+\left(\frac{(\omega-k_\| u_j)}{k_\|\Psi_{T_{\|j}}}\right)Z_2^{(r,q)}(\xi_j)-AGC_3\frac{T_{\perp j}}{T_{\|j}}$$

$$\left.\left.-\left(\frac{T_{\perp j}}{T_{\|j}}-1\right)\xi_j Z_3^{(r,q)}(\xi_j)-\left(\frac{(\omega-k_\| u_j)}{k_\|\Psi_{T_{\|j}}}\right)Z_3^{(r,q)}(\xi_j)\right\}\right] \quad (7)$$

where $= \frac{q(r+1)(q-1)^q}{(q+qr-1)}$, $G=(q-1)^q$,

$$C_1 = \int_{-\infty}^{\infty}\left[1+\frac{1}{q-1}(s)^{2(1+r)}\right]^{-q}ds \quad (8)$$

$$C_2 = \int_{-\infty}^{\infty}ds\, s^{2-2q-2qr}\,{}_2F_1\left[q+1,q-\frac{1}{1+r},q+\frac{r}{1+r},-(q-1)(s)^{-2(r+1)}\right] \quad (9)$$

$$C_3 = \int_{-\infty}^{\infty}s^{2-2q-2qr}\,{}_2F_1\left[q+1,q,q+1,-(q-1)(s^2)^{-(r+1)}\right]ds \quad (10)$$

$$Z_1^{(r,q)} = A\int_{-\infty}^{\infty}\frac{1}{(s-\xi_j)}\left[1+\frac{1}{q-1}(s^2)^{r+1}\right]^{-q}ds \quad (11)$$

$$Z_2^{(r,q)}(\xi_j) = AB\frac{\int_{-\infty}^{\infty}s^{2-2q-2qr}}{(s-\xi_j)}\,{}_2F_1$$

$$\times\left[q+1,q-\frac{1}{1+r},q+\frac{r}{1+r},-(q-1)(s)^{-2(r+1)}\right]ds \quad (12)$$

and

$$Z_3^{(r,q)}(\xi_j) = AG\frac{\int_{-\infty}^{\infty}s^{2-2q-2qr}}{(s-\xi_j)}\,{}_2F_1\left[q+1,q,q+1,-(q-1)(s^2)^{-(r+1)}\right]ds \quad (13)$$

Since we are considering a plasma consisting of cool and hot electrons, and warm electron beam drifting along the magnetic field, respectively, the dispersion relation (7) can be solved assuming $\xi_c = \frac{(\omega-\Omega)}{k_\|\Psi_{T_{\|c}}}\gg 1$, $\xi_h = \frac{(\omega-\Omega)}{k_\|\Psi_{T_{\|h}}}\ll 1$, $\xi_b = \frac{(\omega-\Omega-k_\| u_b)}{k_\|\Psi_{T_{\|b}}}\le 1$ and in the limiting case $\omega\ll\Omega$, we get the general dispersion relation for (r,q) distributed plasma

$$1 = 2\left(\frac{k_\|^2}{k^2}\frac{\omega_{pc}^2}{\omega^2}+\frac{\omega_{pi}^2}{\omega^2}\right)AC_4-\frac{2}{D^2}\left(\frac{1}{k^2\lambda_{Dh}^2}+\frac{1}{k^2\lambda_{Db}^2}\right)AC_1$$

$$-\frac{\omega_{pc}^2}{\Omega^2}\frac{k_\perp^2}{k^2}(ABC_2-AGC_3)-i2A\pi\left[\frac{\omega_{ph}^2}{k^3\Psi_{T_{\|h}}^3}\frac{\omega k}{k_\|}\left(1+\frac{\left(\frac{\omega^2}{k_\|^2\Psi_{T_{\|h}}^2}\right)^{r+1}}{(q-1)}\right)^{-q}\right.$$

$$\left.+\frac{\omega_{pb}^2}{k^3\Psi_{T_{\|b}}^3}\frac{(\omega-k_\| u_b)k}{k_\|}\left(1+\frac{\left(\frac{(\omega-k_\| u_b)^2}{k_\|^2\Psi_{T_{\|b}}^2}\right)^{r+1}}{(q-1)}\right)^{-q}\right] \quad (14)$$

where $k=\sqrt{k_\|^2+k_\perp^2}$,

$$D = \sqrt{\frac{3(q-1)^{-1/(1+r)}\Gamma\left[q-\frac{3}{2+2r}\right]\Gamma\left[\frac{3}{2+2r}\right]}{\Gamma\left[q-\frac{5}{2+2r}\right]\Gamma\left[\frac{5}{2+2r}\right]}} \quad (15)$$

and

$$C_4 = \int_{-\infty}^{\infty}s^2\left[1+\frac{1}{q-1}(s)^{2(1+r)}\right]^{-q}ds \quad (16)$$

In the above dispersion relation (14) contributions from hot electrons and warm electron beam in the real part of the plasma dispersion function have not been taken and retained only $n=0$ terms in the imaginary part which is true for the condition $\omega\ll\Omega$ and $|u_b|\ll\Psi_{T_{\|b}}$. Upon separating the dispersion relation (14) into real and imaginary parts, we can write real frequency and damping/growth rate, respectively as

$$\frac{\omega^2}{\omega_{pe}^2} = k^2\lambda_{Dc}^2\left[\frac{2AC_4D^2\left(\frac{n_c}{n_e}\cos^2\theta\right)}{\left(k^2\lambda_{Dc}^2D^2+\left(\frac{T_{\|c}}{T_{\|h}}\frac{n_h}{n_c}+\frac{T_{\|c}}{T_{\|b}}\frac{n_b}{n_c}\right)2AC_1-(ABC_2-AGC_3)\frac{\omega_{pc}^2}{\Omega^2}k^2\lambda_{Dc}^2D^2\sin^2\theta\right)}\right] \quad (17)$$

$$\frac{\gamma}{\omega_{pe}} = \frac{\pi\left(\omega/\omega_{pe}\right)^4 \left(\frac{n_e}{n_c}\right)^{\frac{1}{2}} \left(\frac{n_h}{n_c}\right) \left(\frac{T_{\|c}}{T_{\|h}}\right)^{\frac{3}{2}}}{2C_4 D^3 k^3 \lambda_{Dc}^3 \cos\theta \left(\frac{n_c}{n_e}\cos^2\theta\right)} \left[\left\{1 + \frac{1}{q-1}\left(\frac{\left(\omega/\omega_{pe}\right)^2}{k^2\lambda_{Dc}^2}\frac{1}{D^2\cos^2\theta}\frac{n_e}{n_c}\frac{T_{\|c}}{T_{\|h}}\right)^{r+1}\right\}^{-q} + \left(\frac{n_b}{n_h}\right)\left(\frac{T_{\|c}}{T_{\|h}}\right)^{3/2}\left(1 - \frac{\left(u_b/v_{t_{\|c}}\right)\cos\theta\, k\lambda_{Dc} D}{\left(\omega/\omega_{pe}\right)}\sqrt{\frac{n_c}{n_e}}\right)\right.$$

$$\left. \times \left\{1 + \frac{1}{q-1}\left(\frac{\left(\omega/\omega_{pe}\right)^2}{k^2\lambda_{Dc}^2}\frac{1}{D^2\cos^2\theta}\frac{n_e}{n_c}\frac{T_{\|c}}{T_{\|b}}\left(1 - \frac{\left(u_b/v_{t_{\|c}}\right)D\cos\theta\, k\lambda_{Dc}}{\left(\omega/\omega_{pe}\right)}\sqrt{\frac{n_c}{n_e}}\right)^2\right)^{r+1}\right\}^{-q}\right] \tag{18}$$

Here we note that the real frequency is only determined by the cool electrons and the damping/growth rate is determined by the hot electrons and warm electron beam. Furthermore, in order to obtain electron acoustic instability, we found that following conditions which must be true simultaneously.

and

$$\sqrt{\frac{n_c}{n_e}}\frac{u_b}{v_{t_{\|c}}}\cos\theta\, k\lambda_{Dc} > \frac{\omega}{\omega_{pe}} \tag{19}$$

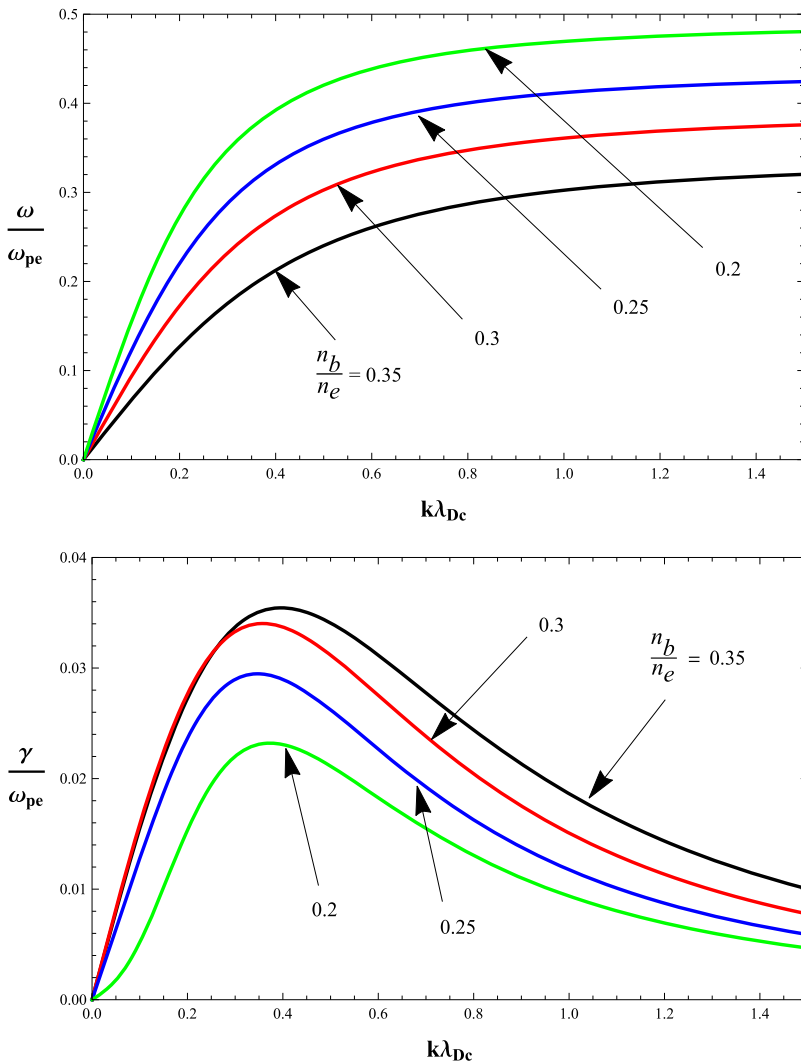$$\frac{u_b}{v_{t_{\|c}}} > U' \tag{20}$$

FIG. 2. Real frequency (upper panel) and growth rate (lower panel) of the electron acoustic instability against the normalized wave number for different ratios of beam to total electron density n_b/n_e (black = 0.35, red = 0.30, blue = 0.25, green = 0.20). Here $\omega_{pc}/\Omega = 0.2$, $\frac{u_b}{v_{t_{\|c}}} = 5$ and the other parameters are the same as in Fig. 1.

where U′ is the critical beam velocity given as

$$
U' = \frac{(\omega/\omega_{pe})}{cos\theta \, k\lambda_{Dc}} \sqrt{\frac{n_e}{n_c}} \left[1 + \left(\frac{n_h}{n_b}\right)\left(\frac{T_{\parallel b}}{T_{\parallel h}}\right)^{3/2} \right.
$$

$$
\left. \times \left[1 + \frac{1}{q-1}\left(\frac{(\omega/\omega_{pe})^2}{k^2\lambda_{Dc}^2} \frac{1}{D^2 cos^2\theta} \frac{n_e}{n_c} \frac{T_{\parallel c}}{T_{\parallel h}} \right)^{r+1} \right]^{-q} \right]
$$

IV. NUMERICAL RESULTS

Broadband electrostatic noise (BEN) have been observed in the Earth's magnetosphere by various satellites, such as Viking observations from auroral region show that T_b = 50 eV, $\frac{n_c}{n_e}$ = 0.15, $\frac{n_h}{n_e}$ = 0.55, $\frac{n_b}{n_e}$ = 0.3, $\frac{T_c}{T_h}$ = 0.008, $\frac{T_c}{T_b}$ = 0.04,

$\frac{T_b}{T_h}$ = 0.2, where 'e' represents the total electron density,[32,33] DE-1 observations polar cusp region show $\frac{n_c}{n_e}$ = 0.2, $\frac{n_h}{n_e}$ = 0.45, $\frac{n_b}{n_e}$ = 0.35, $\frac{T_c}{T_h}$ = 0.001, $\frac{T_c}{T_b}$ = 0.043, $\frac{T_b}{T_h}$ = 0.23[34] and ISEE observations from plasma sheet boundary layer (PSBL) show $\frac{n_c}{n_e}$ = 0.16, $\frac{n_h}{n_e}$ = 0.79, $\frac{n_b}{n_e}$ = 0.05, $\frac{T_c}{T_h}$ = 0.002, $\frac{T_c}{T_b}$ = 0.1.[35,36] We note that the plasma parameters used in fitting of the observed distribution are very close to the observed parameters given above from different regions of space plasmas. Therefore, we will use the fitting parameters along with the parameters observed from space plasmas in the following figures to depict the actual plasma picture.

Figure 2 shows the real frequency (upper panel) and growth rate (lower panel) of the electron acoustic instability against the normalized wave number for different ratios of beam to total electron density n_b/n_e (black = 0.35, red = 0.30, blue = 0.25, green = 0.20). From Fig. 2 we can see that real frequency increases with the decrease in beam density as real
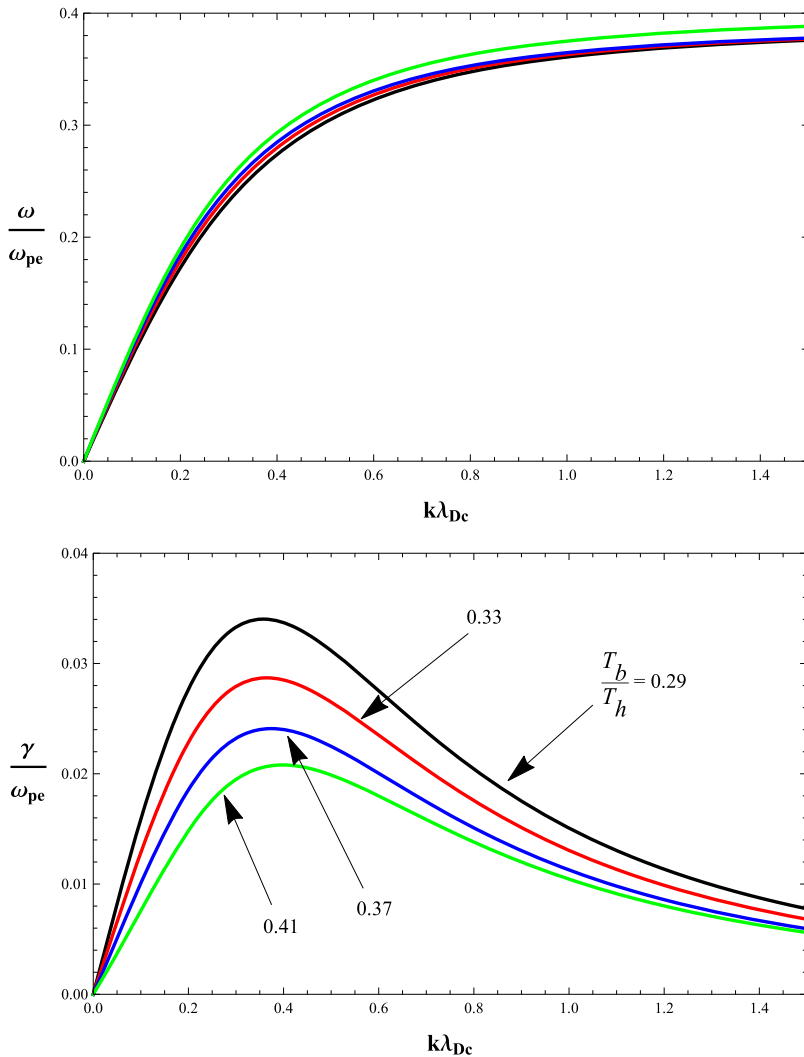

FIG. 3. Real frequency (upper panel) and growth rate (lower panel) of the electron acoustic instability against the normalized wave number for different ratios of beam to hot electron temperature $T_{\parallel b}/T_{\parallel h}$ (black = 0.29, red = 0.33, blue = 0.37, green = 0.41). Here ω_{pc}/Ω = 0.2, $\frac{u_b}{v_{t\parallel c}}$ = 5 and the other parameters are the same as in Fig. 1.

frequency depends upon cool electron population only but growth rate of electron acoustic instability increases with the increase of beam density since instability depends upon beam electron density and more free energy is available to desta-bilize the wave. Figure 3 depicts the real frequency (upper panel) and growth rate (lower panel) of the electron acous-tic instability against the normalized wave number for dif-ferent ratios of beam to hot electron temperature $T_{\parallel b}/T_{\parallel h}$ (black = 0.29, red = 0.25, blue = 0.20, green = 0.16). From Fig. 3 we can see that real frequency slightly increases with the increase of beam temperature but growth rate of elec-tron acoustic instability increases with the decrease of beam temperature.

Figure 4 is plotted for real frequency (upper panel) and growth rate (lower panel) against the normalized wave number for different ratios of cool electron plasma frequency to elec-tron cyclotron frequency ω_{pc}/Ω (black=0.2, red=0.5, blue=0.8, green=1). We can see that real frequency as well as growth rate

of electron acoustic instability increases with the decrease in magnetic field strength. In Fig. 5, real frequency (upper panel) and growth rate (lower panel) is plotted against the normalized wave number for different angles of propagation θ (black = 0, red = 30, blue = 60, green = 85). We can see that real frequency as well as growth rate of electron acoustic instability increases when angle of propagation decreases and remain maximum for un-magnetized case, i.e. $\theta = 0$. Figure 6 depicts the growth rate plotted against the normalized wave number for different values of beam velocity $\frac{u_b}{v_{t_{\parallel c}}}$ (black = 2, red = 3, blue = 5, green = 7). We can see that growth rate of electron acoustic insta-bility increases with the increase of beam velocity, however growth is obtained for all wave numbers when $\frac{u_b}{v_{t_{\parallel c}}} > 3$.

Figure 7 depicts the maximum growth rate plotted against the beam velocity for different values of beam to hot elec-tron temperature ratios $T_{\parallel b}/T_{\parallel h}$ (black = 0.29, red = 0.33, blue = 0.37, green = 0.41). We can see that maximum growth rate of
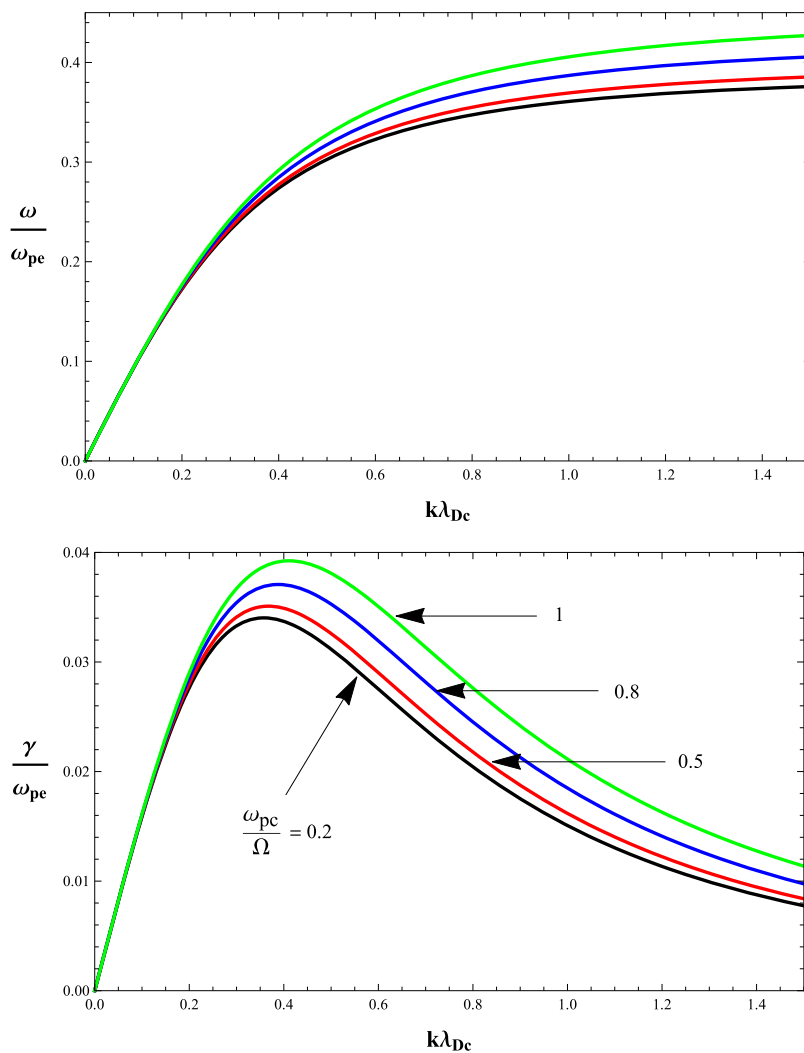

FIG. 4. Real frequency (upper panel) and growth rate (lower panel) against the normalized wave number for dif-ferent ratios of cold electron plasma frequency to electron cyclotron frequency ω_{pc}/Ω (black=0.2, red=0.5, blue=0.8, green=1). Here $\frac{u_b}{v_{t_{\parallel c}}} = 5$ and the other parameters are the same as in Fig. 1.
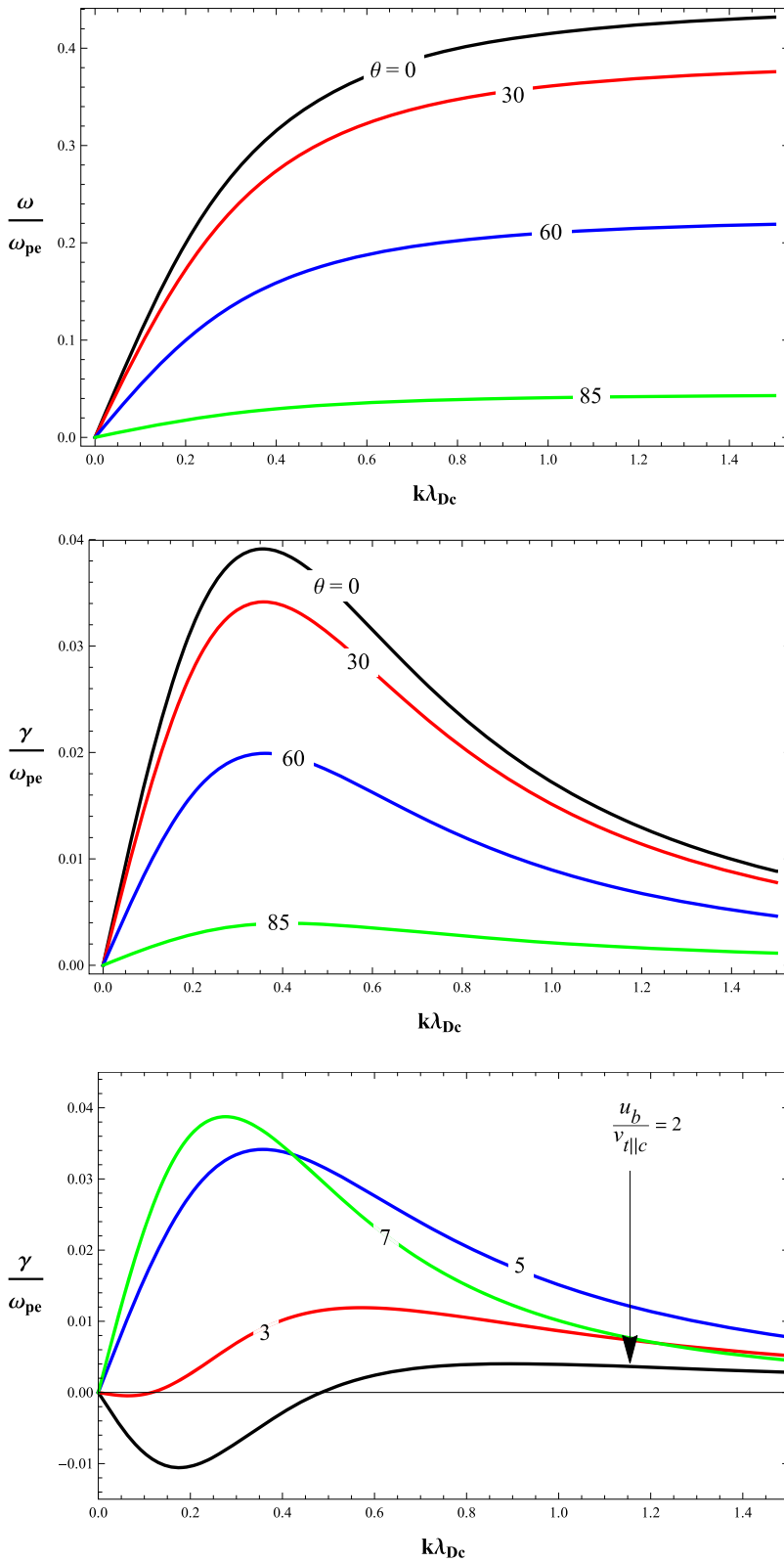
FIG. 5. Real frequency (upper panel) and growth rate (lower panel) is plotted against the normalized wave number for different angles of propagation θ (black = 0°, red = 30°, blue = 60°, green = 85°). Here $\omega_{pc}/\Omega = 0.2$, $\frac{u_b}{v_{t\parallel c}} = 5$ and the other parameters are the same as in Fig. 1.

FIG. 6. Growth rate plotted against the normalized wave number for different values of beam velocity $\frac{u_b}{v_{t\parallel c}}$ (black = 2, red = 3, blue = 5, green = 7). Here $\omega_{pc}/\Omega = 0.2$ and the other parameters are the same as in Fig. 1.
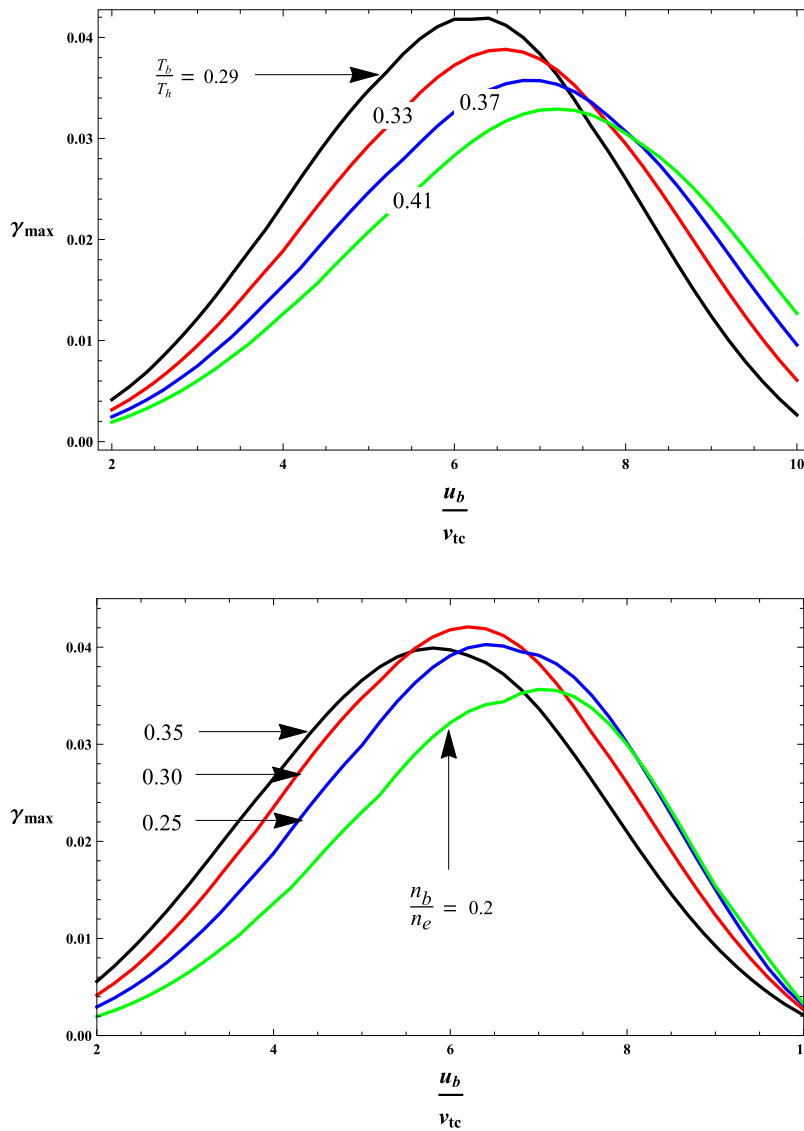
FIG. 7. Maximum growth rate plotted against the beam velocity for different values of beam to hot electron temperature ratios $T_{\|b}/T_{\|h}$ (black = 0.29, red = 0.33, blue = 0.37, green = 0.41). The other parameters are the same as in Fig. 3.

FIG. 8. Maximum growth rate plotted against the beam velocity for different values of beam to total electron density ratios n_b/n_e (black = 0.35, red = 0.3, blue = 0.25, green = 0.2). The other parameters are the same as in Fig. 2.

electron acoustic instability first increases with the decrease of beam temperature for beam velocities $\frac{u_b}{v_{t\|c}} < 7$ but then decreases with the beam temperature for beam velocities $\frac{u_b}{v_{t\|c}} > 7$. Figure 8 depicts the maximum growth rate plotted against the beam velocity for different values of beam to total electron density ratios n_b/n_e (black = 0.35, red = 0.3, blue = 0.25, green = 0.2). We can see that maximum growth rate of electron acoustic instability first increases and then decreases with the decrease of beam density.

Threshold beam velocity, above which electron acoustic instability could be produced, is plotted against the beam to hot electron temperature ratio $T_{\|b}/T_{\|h}$ for different values of beam to total electron density ratios $\frac{n_b}{n_e}$ (black = 0.35, red = 0.30, blue = 0.25, green = 0.20) in Fig. 9. We can note that threshold value of beam velocity increases with the beam

temperature and as the beam density decreases threshold value of the beam velocity increases. Figure 10 is plotted for threshold beam velocity versus beam to total electron density $\frac{n_b}{n_e}$ for different values of beam to hot electron temperature ratios $T_{\|b}/T_{\|h}$ (black = 0.08, red = 0.25, blue = 0.41, green = 0.66). We can see that threshold value of beam velocity decreases with the beam density and as the beam temperature increases threshold value of the beam velocity also increases. Figure 11 is plotted to show a comparison between the real frequencies and growth rates for generalized (r, q) distribution and its limiting form such as kappa and Maxwellian distributions. We can see that real frequency and growth rate remains higher for (r, q) distribution and lowest for kappa distribution, where as Maxwellian values remain in between the values of other two distributions.
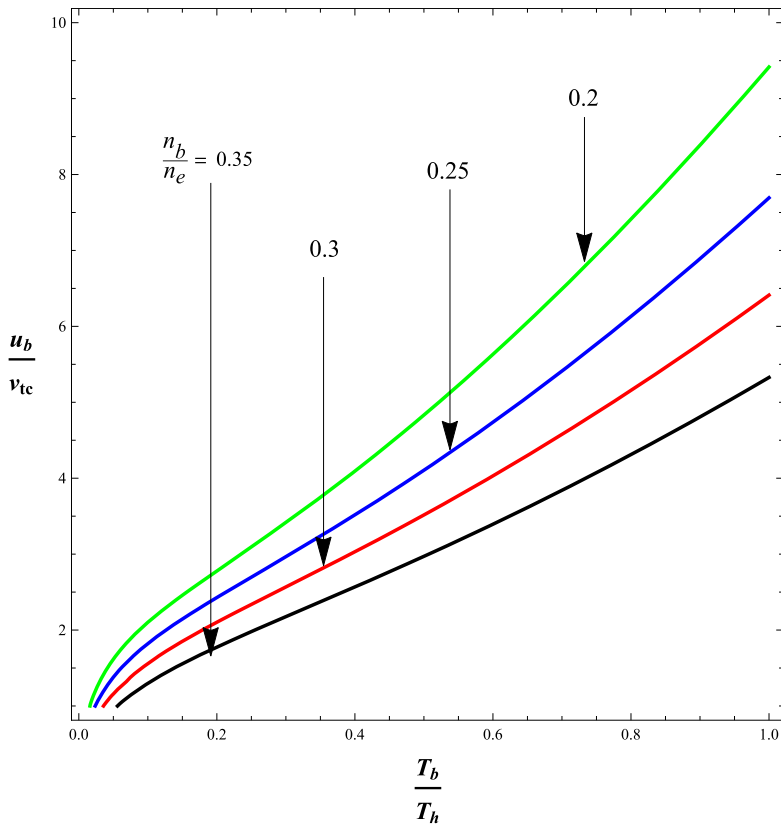
FIG. 9. Threshold beam velocity versus beam to hot electron temperature ratio $T_{\parallel b}/T_{\parallel h}$ for different ratios of beam to total electron number density $\frac{n_b}{n_e}$ (black = 0.35, red = 0.30, blue = 0.25, green = 0.20).
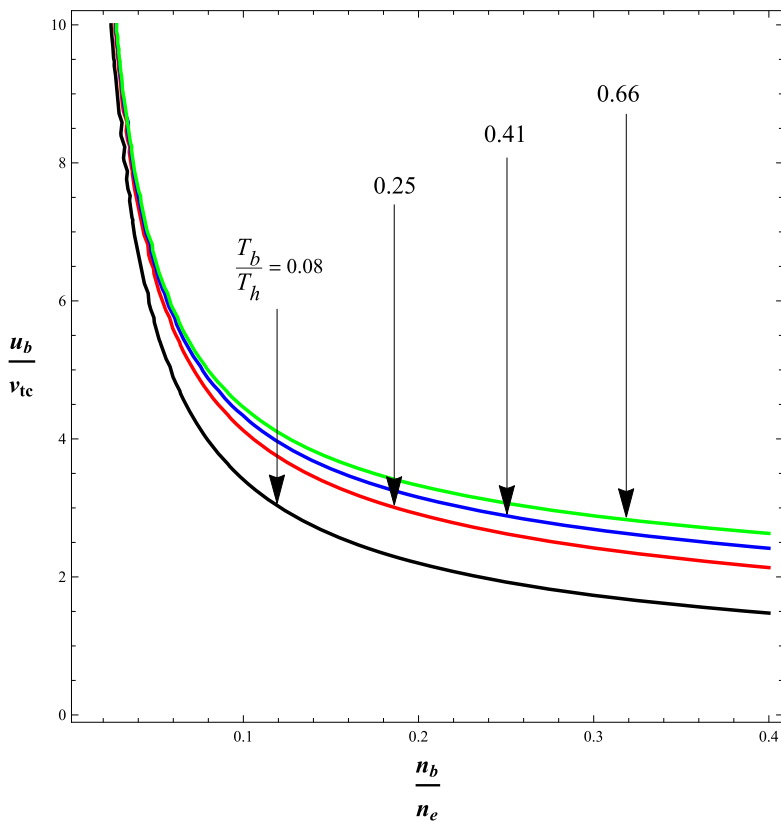

FIG. 10. Threshold beam velocity versus beam to total electron number density $\frac{n_b}{n_e}$ for different values of beam to hot electron temperature ratios $T_{\parallel b}/T_{\parallel h}$ (black = 0.08, red = 0.25, blue = 0.41, green = 0.66).
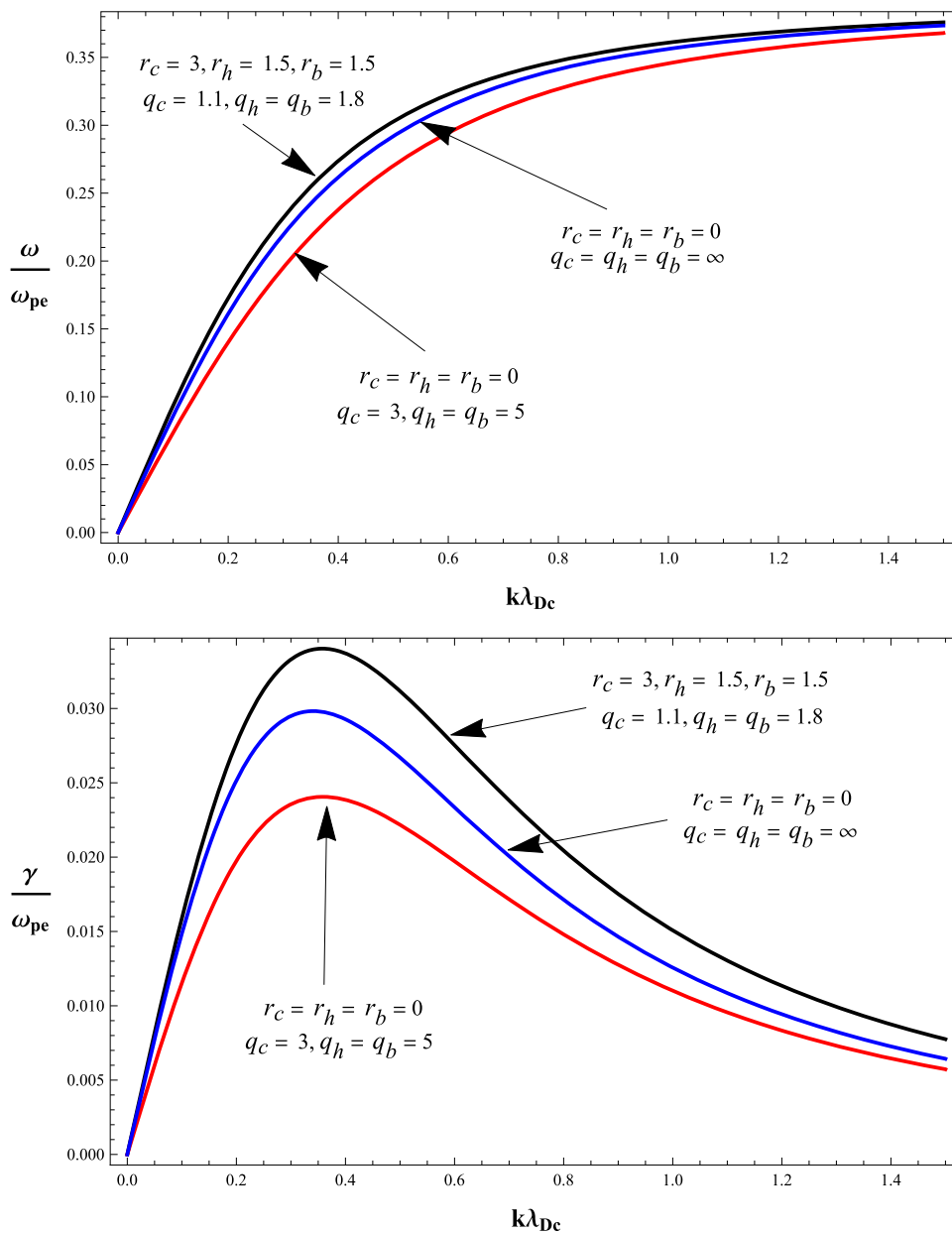
FIG. 11. Comparison of the real frequencies and growth rates for the Maxwellian, kappa and generalized (r,q) distributions.

V. DISCUSSION AND CONCLUSION

We have investigated the electron acoustic instability in magnetized four component plasma with non-Maxwellian generalized (r, q) distribution function. In literature electron acoustic instability has been studied mostly in unmagnetized plasma (results are valid only for the magnetic field direction) and rarely in magnetized plasma but with ideal Maxwellian distribution function.[37] In this paper for the first time, by fitting the observed electron velocity distribution with the generalized (r, q) distribution, we have investigated the obliquely

propagating electron acoustic instability with observed distribution. Furthermore, a comparison of (r, q) distribution results with kappa and Maxwellian results has also presented.

In this study, we considered the strongly magnetized case for which $\frac{\Omega_e}{\omega_{pc}} > 1$ and investigated the effects of beam density, beam temperature, beam velocity and propagation angle on the real frequency and growth rate of the electron acoustic instability. For numerical purposes, fitting parameters along with the observed parameters from different regions of space plasmas have been chosen to present a complete plasma scenario. It has been found that an increase in propagation angle

leads to decrease the magnitude of both real frequency and growth rate. The effect of electron beam density has been studied by varying the ratio n_b/n_e and found that large beam density enhance the electron acoustic instability, same was observed for BEN in polar cusp and auroral region.[18] It is also found that increase in beam temperature suppresses the instability, which shows that when wave grows to large amplitudes it scatters and heat the beam particles, and hence instability regulates itself. It is shown that increase in beam velocity above a critical value increases the growth rate of the instability for all values of wave numbers, i.e. at threshold Landau damping eventually goes to zero and further increase in beam velocity increases the growth. We have also found that real frequency and growth rates are higher for unmagnetized plasma than the magnetized plasma.

If we consider Fig. 2, n_b/n_e varies from 0.35 to 0.2, n_c/n_e varies from 0.15 to 0.3, $n_h/n_e = 0.5$, $u_b/v_{t\|c} = 5$, and fitting in Fig. 1 where $T_{\|c} = 3$ eV, $T_{\|h} = 122$ eV and $T_{\|b} = 35$ eV, we found that real frequency varies from 3.2 kHz to 4.8 kHz (Fig. 2 upper panel) and maximum growth ranges from 296 ms to 557 ms (Fig 2 lower panel). This is in agreement with the observation of EAWs from Auroral region with 3 kHz and from polar cusp region with 4-10 kHz. Similarly, if we consider Fig. 3 where $T_{\|b}$ is varied from 20 to 35 eV, $T_{\|c}$ from 0.5 to 3 eV, $T_{\|h} = 122$ eV, $u_b/v_{t\|c} = 5$, and Fig. 1 where $n_b/n_e = 0.3$, $n_c/n_e = 0.2$ and $n_h/n_e = 0.5$, we found that maximum growth varies from 330 ms to 748 ms (Fig. 2 lower panel) and real frequency varies from 3.6 kHz to 4.5 kHz (Fig. 3 upper panel) which is closely related to observations of EAWs from PSBL with 3-4 kHz and from Polar cusp region with 4-10 kHz. In we consider the numerical values of parameters used in Fig. 11, values of spectral indices r and q for (r,q) distribution from fitting, spectral indices for Kappa distribution as $r_c = r_h = r_b = 0$ and $q_c = 3$, $q_h = 5$, $q_b = 5$ and for Maxwellian $r_c = r_h = r_b = 0$ and $q_c = q_h = q_b = \infty$, respectively, for (r,q) distribution the maximum growth and real frequency come out to be 330 ms and 3.6 kHz, for kappa distribution 467 ms and 3.1 kHz and for Maxwellian distribution 375 ms and 3.4 kHz, respectively. Thus a comparison between the (r,q) distribution and other distributions showed that when we use realistic parameters and employed observed distribution, real frequency and growth rate remain higher than the Maxwellian or kappa values. Therefore, in this paper, by employing observed distribution function, we have presented a realistic plasma picture and showed that in actual situations frequency and growth rate of EA instability exhibits significantly different behavior from the situations where ideal distributions have been employed.

REFERENCES

[1] W. C. Feldman, R. C. Anderson, S. J. Bame, J. T. Gosling, and R. D. Zwickl, J. Geophys. Res. **88**, 9949, https://doi.org/10.1029/ja088ia12p09949 (1983).

[2] M. F. Thomsen, H. C. Barr, S. P. Gary, W. C. Feldman, and T. E. Cole, J. Geophys. **88**, 3035, https://doi.org/10.1029/ja088ia04p03035 (1983).

[3] K. Watanabe and T. Taniuti, J. Phys. Soc, Jpn **43**, 1819 (1977).

[4] R. L. Tokar and S. P. Gary, Geophys. Res. Lett. **11**, 1180, https://doi.org/10.1029/gl011i012p01180 (1984).

[5] D. A. Gurnett and L. A. Frank, J. Geophys. Res. **83**, 58, https://doi.org/10.1029/ja083ia01p00058 (1978).

[6] E. Marsch, J. Geophys. Res. **90**, 6327, https://doi.org/10.1029/ja090ia07p06327 (1985).

[7] M. Ashour-Abdalla and H. Okuda, Geophys. Res. Lett. **13**, 366, https://doi.org/10.1029/gl013i004p00366 (1986).

[8] C. S. Lin, D. Winske, and R. L. Tokar, J. Geophys. Res. **90**, 8269, https://doi.org/10.1029/ja090ia09p08269 (1985).

[9] I. Roth and M. K. Hudson, J. Geophys. Res. **91**, 8001, https://doi.org/10.1029/ja091ia07p08001 (1986).

[10] C. S. Lin, D. Winske, and R. L. Tokar, J. Geophys. Res. **92**, 7569, https://doi.org/10.1029/ja092ia07p07569 (1987).

[11] D. A. Gurnett, L. A. Frank, and R. P. Lepping, J. Geophys. Res. **81**, 6059, https://doi.org/10.1029/ja081i034p06059 (1976).

[12] D. Schriver and M. Ashour-Abdalla, J. Geophys. Res. **92**, 5807, https://doi.org/10.1029/ja092ia06p05807 (1987).

[13] S. P. Gary and R. L. Tokar, Phys. Fluids **28**, 2439 (1985).

[14] S. P. Gary, Phys. Fluids **30**, 2745 (1987).

[15] R. Bharuthram, J. Plasma Phys. **46**, 1 (1991).

[16] R. Bharuthram, Astrophys. Space Sci. **202**, 337 (1993).

[17] M. A. Hellberg, R. L. Mace, R. J. Armstrong, and G. Karlstad, J. Plasma Phys. **64**, 433 (2000).

[18] L. N. Mbuli, S. K. Maharaj, and R. Bharuthram, Phys. Plasmas **20**, 122115 (2013).

[19] M. D. Montgomery, J. R. Asbridge, and S. J. Bame, J. Geophys. Res. **75**, 1217, https://doi.org/10.1029/ja075i007p01217 (1970).

[20] W. C. Feldman, R. C. Anderson, S. J. Bame, S. P. Gary, J. T. Gosling, D. J. McComas, M. F. Thomsen, G. Paschmann, N. Sckopke, C. T. Russsell, and M. M. Hoppe, Phys. Res. Lett. **49**, 199 (1982).

[21] Y. Asano, R. Nakamura, I. Shinohara, M. Fujimoto, T. Takada, W. Baumjohann, C. J. Owen, A. N. Fazakely, A. Runov, T. Nagai, E. A. Lucek, and H. Reme, J. Geophys. Res. **113**, A01207, https://doi.org/10.1029/2007ja012461 (2008).

[22] W. Masood and S. J. Schwartz, J. Geophys. Res. **113**, A01216, https://doi.org/10.1029/2007ja012715 (2008).

[23] G. K. Parks, L. Lee, A. Teste, M. Wilber, N. Lin, P. Canu, I. Dandouras, H. Reme, S. Y. Fu, and M. L. Goldstein, Phys. Plasmas **15**, 080702 (2008).

[24] H. Khalilpour, Astrophys. Space Sci. **361**, 271 (2016).

[25] M. J. Lee and Y. D. Jung, Phys. Plasmas **25**, 053704 (2018).

[26] W. F. El-Taibany, A. Atteya, and S. K. El-Labany, Phys. Plasmas **25**, 083704 (2018).

[27] S. Zaheer and P. H. Yoon, Astrophys. J. **775**, 108 (2013).

[28] M. N. S. Qureshi, W. Nasir, W. Masood, P. H. Yoon, H. A. Shah, and S. J. Schwartz, J. Geophys. Res.: Space Phys. **119**, 10059, https://doi.org/10.1002/2014ja020476 (2014).

[29] W. Masood, S. J. Schwartz, M. Maksimovic, and A. N. Fazakerley, Ann. Geophys. **24**, 1725 (2006).

[30] A. D. Johnstone, C. Alsop, P. J. Carter, A. J. Coates, A. J. Cooker, A. N. Fazakerley, M. Grande, R. A. Gowen, C. Gurgiolo, B. K. Hancock, B. Narheim, A. Preece, P. H. Sheather, J. D. Winningham, and R. D. Woodliffe, Space Sci. Rev. **79**, 351 (1997).

[31] N. A. Krall and A. W. Trivlepiece, *Principles of Plasma Physics*, McGraw-Hill, New York, p. 376 (1973).

[32] N. Dubouloz, R. Pottellette, M. Malingre, G. Holmgren, and P. A. Lindqvist, J. Geophys. Res. **96**, 3565, https://doi.org/10.1029/90ja02355 (1991).

[33] N. Dubouloz, R. A. Treumann, R. Pottelette, and M. Malingre, J. Geophys. Res. **98**, 17415, https://doi.org/10.1029/93ja01611 (1993).

[34] C. S. Lin, J. L. Burch, S. D. Shawhan, and D. A. Gurrnett, J. Geophys. Res. **89**, 925, https://doi.org/10.1029/ja089ia02p00925 (1984).

[35] G. K. Parks, J. Geophys. Res. **89**, 8885 (1984).

[36] T. G. Onsager, M. F. Thomsen, R. C. Elphic, J. T. Gosling, R. R. Anderson, and G. Kettmann, J. Geophys. Res. **98**, 15509, https://doi.org/10.1029/93ja00921 (1993).

[37] A. Sooklal and R. L. Mace, Phys. Plasmas **11**, 1996 (2004).